Scientia Iranica B (2014) 21(4), 1390–1402

SCIENTIA
IRANICA

Sharif University of Technology
Scientia Iranica
Transactions B: Mechanical Engineering
www.scientiairanica.com

Modeling active micromixers with multiple microstirrers using smoothed particle hydrodynamics

A. Jafarian[a,*], **A. Pishevar**[a] **and M.S. Saidi**[b]

a. *Department of Mechanical Engineering, Isfahan University of Technology, P.O. Box 84156-83111, Isfahan, Iran.*
b. *Center of Excellence in Energy Conversion and Department of Mechanical Engineering, Sharif University of Technology, Tehran, Iran.*

Received 8 October 2012; received in revised form 6 September 2013; accepted 4 November 2013

KEYWORDS
Smoothed particle hydrodynamics;
Micromixer;
Microstirrer;
Mixing chamber;
Molecular diffusion.

Abstract. The smoothed particle hydrodynamics method is used to explore the effects of design parameters on the mixing efficiency of two types of active micromixer. First, the complex flow field and the mixing process of two separated fluids in a square mixing chamber with nine symmetric microstirrers are simulated. The influence of design parameters, such as the microstirrer rotation arrangement and the angular velocity of the microstirrer, on the mixing performance, is investigated. The mixing index parameter on ten control points is calculated and the average mixing index is compared for different cases. Simulations illustrate that the rotation arrangement of microstirrers is a key parameter in the mixing process. Then, a parametric study is performed for a horizontal and a Y-shaped active micromixer, where the influence of length, angular velocity, rotation or oscillation movement of the microstirrer, inlet Reynolds number, and inlet stream angle is investigated. It is also illustrated that the inlet Reynolds number and the Struhal number are prominent parameters that affect the mixing efficiency of this type of active micromixer.

1. Introduction

In recent years, microfluidic systems have advanced significantly, and many biochip systems have been developed over a wide range, from chemical analysis to drug delivery, DNA hybridization, enzyme reactions, and sequencing or synthesis of nucleic acids [1-3]. Fluid mixing is a vital process in many procedures performed by microchips. Consequently, the rapid mixing and response time of these devices are essential performance parameters and obviously illustrate the importance of micromixer design [4]. However, in these devices, the geometry dimensions are usually rather small and, so, typically, the flow regime is constrained to low Reynolds numbers [5]. Generally, a mixing process is accomplished by three mechanisms: molecular diffusion, bulk diffusion and vortex diffusion. The dominant Reynolds numbers in micromixers are of the order of unity or less than 1, which are representative of laminar flow or creeping flow in a microfluidic system. Hence, in both cases, vortex diffusion is negligible and molecular diffusion becomes the main mixing mechanism for these devices [6].

Many different mixing techniques have been presented recently to overcome the slow progress of the mixing process by molecular diffusion in micromixers. Generally, micromixers can be classified into passive and active micromixers. Passive micromixers employ special geometries to increase the contact surface between the mixing fluids, and the mixing process develops through chaotic advection. Glatzel et al. [7] used four computational fluid dynamics software programs (CFD-ACE, CFX, Flow 3D and Fluent) to simulate a multi lamination micromixer, flow pattern on a

---

*. *Corresponding author. Tel: +98 9127320485;*
Fax: +98 311 3912628
E-mail address: ajafarian@me.iut.ac.ir (A. Jafarian)

rotating platform, bubble dynamics in a microchannel and a TopSpot droplet generator for microarray printing. Tofteberg et al. [8] and Park J.M. et al. [6] used lamination in the planar channel to increase the mixing efficiency of the micromixer at low Reynolds numbers (Re < 10), and the rotation of the flow field is obtained by patterning the channel bed with grooves. Cortes-Quiroz et al. [9] explored the effects of staggered herringbone geometry on the mixing improvement for Re $= 1$ and Re $= 10$. Chen et al. [10] also investigated the performance of a folding flow micromixer in the Stokes flow regime computationally and experimentally for different values of Peclet number up to 10000, and where the Reynolds number is much lower than unity. Tung and Yang [11] analyzed a chaotic mixing in a Circulation-Disturbance Micromixer (CDM) at Re $= 1$, numerically and experimentally. Furthermore, Kang et al. [12] used periodic and aperiodic sequences of mixing protocols in a barrier embedded micromixer to produce chaotic mixing in a wide range of Reynolds numbers from 0.01 to 30. On the other hand, active micromixers use an external disturbance, such as pressure, temperature, electrohydrodynamics or acoustics, for mixing in low Reynolds numbers [13,14]. In the case of active micromixers, Muller et al. [15] optimized a transverse momentum micromixer numerically at Re $= 5$. Park J.Y. et al. [16] used the Lattice Boltzmann method to model a straight micromixer with a microstirrer for various values of Peclet number, from 50 to 500. Lu et al. [17] investigated the mixing process in a mixing chamber with a 3×3 mixer array, which is placed in the middle of the $2000\times2000\times50$ μm square chamber, and a straight micromixer with a size of $7000\times750\times70$ μm using a magnetic microstirrer at a very low Reynolds number, and the transient solution of the rotating microstirrer is presented. Wang et al. [18] simulated a rapid magnetic particle driven by a micromixer that uses a magnetic actuation force in the mixing channel, in which the alternating actuation of magnetic particles suspended in the fluid enhance the mixing process in the microchannel.

Optimization of the geometry and operating condition of microfluidic systems before the manufacturing process, especially micromixers, is an essential procedure. Furthermore, the expenditure of experimental methods in order to find the optimum case is high. Nowadays, interest in numerical analysis of microdevices has increased, due to the difficulties of measuring physical properties in small miniature scale. However, calculation of a deformable region, like an active micromixer with a moving stirrer, is still a challenge in the area of computational fluid dynamics. For problems involving small deformations in the boundaries, it is possible to use conventional grid-based FDM/FVM or FEM methods to solve governing equations on a deformable grid. However, when domain deformation becomes large, for example, in the moving boundaries or free surface flows, the calculation will ultimately fail due to the mesh associated problems. For these reasons, research communities have developed a strong interest in the development of robust mesh free methods for deformable boundary problems. In many applications of this kind, mesh free methods are superior to their conventional grid-based FDM/FVM or FEM counterparts. These methods provide an accurate and stable numerical solution for integral equations or partial differential equations with a set of arbitrary distributed nodes or particles, without using any mesh that provides the connectivity of these particles [19]. Among different mesh free methods, the SPH method has been used more extensively for problems in fluid and structural dynamics. The SPH is a fully Lagrangian method, which was originally developed for astrophysical applications [20-21], then, extended successfully to a wide range of applications, such as free surface flows, deformable boundaries, moving interface and large deformations in impact problems [19]. The foundation of the SPH method is an interpolation theory. The conservation laws of continuum fluid dynamics are transferred into integral equations through the use of an interpolation function that gives the kernel estimate of the field variable at a point or particles [22]. In recent years, the SPH method has been developed in many fields of fluid mechanics problems and many algorithms have been presented for increasing the efficiency of this method. For instance, Ferrari et al. [23] parallelized the SPH code using a standard Message Passing Interface (MPI) to simulate the free surface flow. Furthermore, Espanol and Revenga [24] combined the SPH with the DPD (Dissipative Particle Dynamics) method that solved the Navier-Stokes equation and has the superior feature of the DPD method in modeling mesoscale phenomena.

The objective of this paper is to simulate the flow field that arises in an active micromixer and provide proper insight into the performance and effects of various parameters, such as stirrer geometry and rotational speed during the mixing process.

2. Governing equations and numerical method

2.1. Governing equations

The fluid is taken to be incompressible and Newtonian and the flow is assumed to be transient. The continuity and momentum equations are given as:

$$\frac{1}{\rho}\frac{D\rho}{Dt}+\nabla.\vec{V}=0, \tag{1}$$

$$\frac{d\vec{V}}{dt}=-\frac{1}{\rho}\nabla P+\nabla.(\nu\nabla\vec{V})+\vec{F}, \tag{2}$$

where ρ, V and P are the density, the velocity vector and the pressure, respectively, and ν is the kinematic viscosity. F denotes the external body force. Furthermore, Fick's law is used in order to calculate the mass diffusion. The unsteady transport equation for the mass concentration of one species is considered as:

$$\frac{DC}{Dt} = \frac{1}{\rho}\nabla.(D\nabla C), \tag{3}$$

where C is the mass concentration of one species in a binary solution, and D is the corresponding mass diffusivity.

2.2. SPH formulation

In SPH, in contrast to classical CFD methods, the fluid equations are solved on a set of particles instead of nodes. SPH particles are not real particles; they have finite mass and volume, and follow their movement and the density. The velocity of these particles is obtained through explicit integration of Newton's second law. Representing dependent variables by the integral interpolant, it can be shown that the density evolution of each particle follows [25]:

$$\frac{d\rho_i}{dt} = \sum_j m_j \vec{v}_{ij}.\nabla W_{ij}, \tag{4}$$

where $v_{ij} = v_i - v_j$ is the difference between the velocities of particle i and particle j, m_j is the particle mass, and ∇W_{ij} represents the gradient of the kernel function, $W(x_i - x_j, h)$. In this work, the quintic spline function is used as the kernel:

$$W(s) = \frac{7}{478\pi}$$
$$\begin{cases} (3-s)^5 - 6(2-s)^5 + 15(1-s)^5 & 0 \le s < 1, \\ (3-s)^5 - 6(2-s)^5 & 1 \le s < 2, \\ (3-s)^5 & 2 \le s < 3, \\ 0 & s \ge 3. \end{cases} \tag{5}$$

$s = \frac{r}{h} = \frac{|x-x'|}{h}$ and r is the distance between two particles at x and x', and h is the smoothing length of the kernel.

The momentum equation in the absence of body force and viscous terms reduces to:

$$\frac{d\vec{v}_i}{dt} = -\sum_j m_j \left(\frac{P_i}{\rho_i} + \frac{P_j}{\rho_j}\right) \nabla W_{ij}. \tag{6}$$

The viscous force model presented by Morris et al. [26] employs an SPH estimation of viscous diffusion, which is similar to an expression used in [27] to model heat conduction. This is a hybrid expression that combines the standard SPH first derivative with the finite difference approximation of a first derivative. This expression conserves the linear momentum exactly. Thus, the momentum equation with viscous term and body force is written as:

$$\frac{d\vec{v}_i}{dt} = -\sum_j m_j \left(\frac{P_i}{\rho_i} + \frac{P_j}{\rho_j}\right) \nabla W_{ij} + \sum_j \frac{m_j(\mu_i + \mu_j)\vec{v}_{ij}}{\rho_i \rho_j} \left(\frac{1}{r_{ij}} \frac{\partial W_{ij}}{\partial r_i}\right) + \vec{F}_i, \tag{7}$$

where μ_i and μ_j are the kinematic viscosities of particles i and j, and F_i is the body force.

The pressure term in Eq. (7) is obtained from an explicit function of local fluid density and, as a result, particles are driven by density gradients. Therefore, in standard SPH, incompressible fluid flow is simulated by assuming that the fluid is slightly compressible and the density fluctuations are limited to within 1% [26]. The equation of state suggested by Batchelor is used to evaluate the pressure [28]:

$$P = P_0 \left[\left(\frac{\rho}{\rho_0}\right)^\gamma - 1\right], \tag{8}$$

where:

$$P_0 = \rho_0 \frac{c^2}{\gamma}.$$

$\gamma = 7$ for water, ρ_0 is the initial density, P_0 is the bulk modulus and c is the speed of sound. c is set to be at least ten times higher than the maximum velocity in the domain.

The SPH discretization of Eq. (3) is similar to the discretization of the viscous term in the momentum equations. Therefore, the rate of change of concentration, C_i, of particle i in the domain, is given by [29]:

$$\frac{dC_i}{dt} = \sum_j \frac{m_j}{\rho_i \rho_j} \frac{4D_i D_j}{(D_i + D_j)} (C_i - C_j) \left(\frac{1}{r_{ij}} \frac{\partial W_{ij}}{\partial r_i}\right). \tag{9}$$

Finally, in order to avoid an unphysical particle motion, the particle position is updated by the XSPH variant velocity, which is emanated from the contribution of the neighboring particles to make the particle move with a velocity near the average velocity of the neighboring particles and, thus, keeping the particles more orderly [19]:

$$\frac{dr_i}{dt} = v_i + \varepsilon \sum_j m_j \frac{v_{ij}}{\rho_{ij}} W_{ij}, \tag{10}$$

where, in most simulations, ε is set to 0.3, and $\rho_{ij} = \frac{\rho_i + \rho_j}{2}$.

The SPH method is an explicit method and, in this research, the predictor-corrector scheme is used for the time integration. In this case, just as in other explicit methods, the CFL condition is used to evaluate the time step size. However, the existence of virtual particles and their fast angular velocity in the middle of the fluid particles cause the time step size to reduce to about an order of magnitude less than that predicted by the CFL condition.

2.3. Boundary conditions

Generally, the SPH implementation of physical boundary conditions is one of the most challenging concepts. Due to their meshless nature, fluid particles may penetrate into the solid region during the integration. Therefore, two basic conditions (no slip and no penetration) should be satisfied on a solid wall, simultaneously. In this work, two types of boundary particle, which are placed at the solid walls with a fixed arrangement, are used for implementation of boundary conditions. The first type is the virtual particle, represented by Monaghan [25]. Virtual particles arrange in a line, right on the solid boundary, and impose a high repulsive force to the particles moving towards the wall, to prevent them from unphysically penetrating through the boundary. When a fluid particle, I, approaches a virtual particle, j, a force is applied along the centerline of these two particles, according to:

$$F_{ij}=\begin{cases} D\left[\left(\frac{r_0}{r_{ij}}\right)^{n_1}-\left(\frac{r_0}{r_{ij}}\right)^{n_2}\right]\frac{x_{ij}}{r_{ij}^2} & \left(\frac{r_0}{r_{ij}}\right)\leq 1 \\ 0 & \left(\frac{r_0}{r_{ij}}\right) \end{cases} \tag{11}$$

where parameters n_1 and n_2 are usually taken as 12 and 6, respectively, and r_0 is the cutoff distance. The coefficient, D, is chosen to be in the same scale of the largest velocity. The other types of boundary particle are called mirror ghost particles. These particles are rearranged in every time step. When a fluid particle enters a region near the boundary, usually within a distance in the order of the smoothing length, h, a ghost particle is located symmetrically on the other side of the boundary. These ghost particles have the same density and pressure as the corresponding real particles but opposite velocity. The ghost particles take part in the force summations and provide the necessary shearing effects of the fluid particles near the surface. Other boundary conditions are inflow and outflow conditions. These conditions are implemented at the inlet and outlet of the channel. For the inflow condition, a region is specified before the boundary in which all physical properties of the particles are kept at constant inlet values. For the outflow condition, the channel is considered to be longer, and at the end of the channel, a region is specified as the outflow region. The size of this region is about several times larger than the smoothing length. When particles enter this region, their velocities are frozen and they move with respect to this velocity. Detailed information about the implementation is presented in [30].

3. Results and discussion

In this section, a parametric study of three types of active micromixer is presented and the influence of effective parameters on the mixing phenomena is investigated. Since the accuracy of the SPH method for diffusion dominant problems has been controversially argued in the literature, diffusion in a semi-infinite plate with a Dirichlet boundary condition is calculated and compared to the analytical solution, as the benchmark.

In this paper, the two fluids are treated as a single phase. Two fluids have different concentrations and the diffusion equation is solved for the particles. Furthermore, the mass of these particles remain constant during the molecular diffusion.

In all simulations, the mixing fluids are considered to be water, with different colors, but with the same physical properties: $\rho = 1000$ (kg/m^3), $\nu = 10^{-6}$ (m^2/s) and $D = 10^{-9}$ (m^2/s). The color of the first fluid is assumed to be white and the second fluid is black, with the corresponding concentration value of $C_0 = 0$ for the white water and $C_1 = 1$ for the black water. Furthermore, in order to evaluate mixing efficiency, the mixing index parameter, D_I, is defined as the standard deviation of the local concentration divided by its mean value:

$$D_I=\sqrt{\frac{1}{N}\sum_1^N\left(\frac{C_i-C_{\text{mean}}}{C_{\text{mean}}}\right)^2}, \tag{12}$$

where N is the number of interest points, C_{mean} is the initial mean concentration and C_i is the local concentration. The smaller the mixing index becomes, the more homogenous the fluid is in the channel. When the mixing index is below 0.2, complete mixing is achieved [16].

Comparing the dimensions of the problems under consideration with the molecular mean free path of water, we realize that the continuum equations and no slip boundary conditions on solid walls are still valid. Furthermore, the other important dimensionless numbers in our problem are Reynolds number, which represents the ratio between momentum and viscous force, and the Peclet number, which is the ratio between the convective mass transfer to the diffusive mass transfer:

$$\text{Re}=\frac{\text{UL}}{\nu}, \tag{13}$$

$$\text{Pe}=\frac{\text{UL}}{D}, \tag{14}$$

where D is the mass diffusivity and L is the characteristic length. The other important parameter for an active micromixer is the Struhal number, which represents the ratio between the residence time of the species and the period of the disturbance [13]:

$$\mathrm{St} = \frac{fL}{U}. \tag{15}$$

3.1. *Diffusion in a semi-infinite plane*

In order to verify the diffusion code, a simple diffusion problem is modeled and the numerical result is compared with the analytical solution. For this example, the computational domain is a square of 1 m length and initial concentration, $C_i = 0$. At $t = 0$, concentration on the left wall is set to $C_s = 0.5$ and concentration increases in the domain by time. In this problem, 2500 (50×50) particles are located uniformly in the domain. This example is similar to a diffusion problem in a semi-infinite plate with a step boundary condition for concentration at the surface, and its analytical solution is given by the error function as:

$$\frac{C(t,x) - C_s}{C_i - C_s} = erf\left(\frac{x}{2\sqrt{\frac{Dt}{\rho}}}\right). \tag{16}$$

The boundary condition on the left wall is satisfied by freezing the concentration of ghost particles to the given value. In this example, the diffusivity coefficient is considered to be $D = 10^{-5}$ (m^2/s).

The variation of concentration in a horizontal cross section of the domain is mapped versus the X coordinate for $t = 1$ s, 4 s and 8 s, (Figure 1). Furthermore, Table 1 illustrates the second norm of error at the corresponding time. As we can see, the SPH results are in close agreement with the analytical solution. This example demonstrates that the diffusion process is modeled properly by the present SPH method.

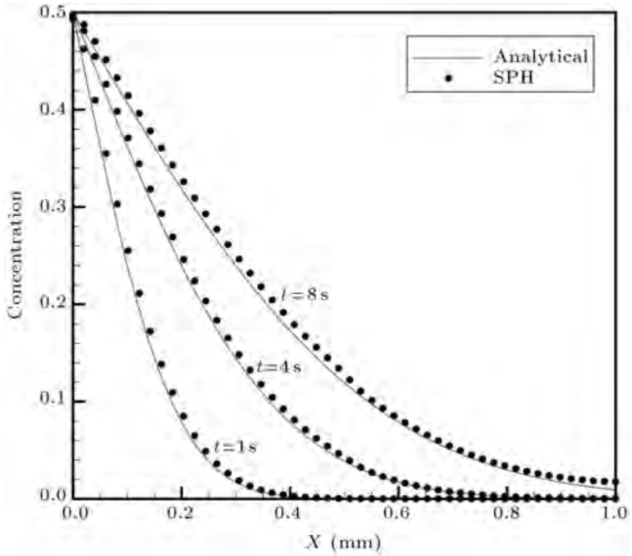

Figure 1. Comparison between analytical and SPH solutions for the diffusion problem.

3.2. *Mixing chamber with 9 micro-stirrers*

The diffusivity coefficient for most real problems is a very small number. Thus, in many practical applications, mixing is accomplished without adequate speed by molecular diffusion. In order to achieve a rapid and effective mixing, it is a common practice to use microstirrers in the chamber. However, the geometrical parameters of the stirrers, their arrangement and rotational speed have significant effects on the mixing process. In this study, we demonstrate how the presented numerical tool can be used to optimize these parameters for an active micromixer. For this reason, we consider the mixing process in a chamber with nine microstirrers arranged symmetrically in the space. A schematic configuration of this example is shown in Figure 2. The chamber is a square of 2000 μm and the length of each microstirrer is considered to be 400 μm. The SPH particles are initially distributed

Table 1. Error norm in terms of elapsed time for the diffusion problem in a semi-infinite plate.

Time	**Error =** $\left[\frac{\sum_1^N \left(C(x)_{\mathrm{SPH}} - C(x)_{\mathrm{Analytic}}\right)^2}{N}\right]^{\frac{1}{2}}$
$t = 1$ s	0.009123887
$t = 4$ s	0.006701568
$t = 8$ s	0.007789181

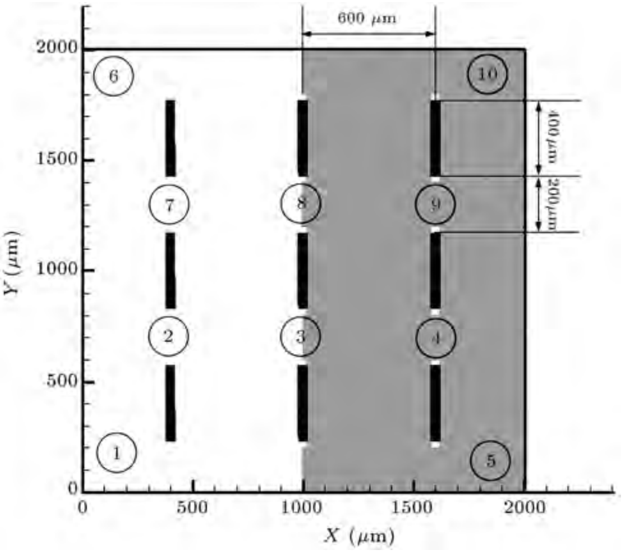

Figure 2. A schematic of the mixing chamber with 9 microstirrers; mixing index is calculated at control points shown by numbers.

on a rectangular 100 × 100 grid with equal spacing in x and y directions. The total number of fluid particles and stirrer virtual particles is 9820 and 180, respectively. The initial spacing between the particles is $dx = dy = 4 \times 10^{-5}$ and, also, the time step size used in this simulation is $dt = 10^{-5}$. Two fluids are initially separated and mixing starts suddenly by stirring the chamber. Mirror ghost particles are used to apply boundary conditions at the chamber walls, and the microstirrers are modeled with virtual particles. The influence of three different angular velocities and three types of rotating arrangement is investigated. As Figure 2 shows, the mixing index parameter is evaluated at 10 control points in the chamber.

3.2.1. First rotation arrangement

In the first rotation arrangement, all microstirrers rotate counter clockwise, and the angular velocity of these microstirrers is constant and $\omega = 200$ rpm. Figure 3 shows sequential snapshots of concentration contours in the mixing chamber at $t = 0$, 0.06 s, 0.1 s, 0.2 s, 0.3 s, 0.5 s, 1 s, 2 s, 5 s, 10 s, 15 s and 20 s. As deduced from this figure, after 20 seconds, two fluids are completely mixed and a homogenous gray color is obtained within the chamber. The mixing index for control points 6, 7 and 8 are illustrated in Figure 4, as a function of non-dimensional time, $\tilde{t}$, where:

$$\tilde{t} = \frac{t \times \nu}{(L_{\text{Stirrer}})^2}.$$

The mixing indices show a harmonic variation with descending amplitude for these points and finally converge to zero after $120\tilde{t}$, which means a complete homogenous mixture. When all microstirrers rotate counter clockwise, approximately, the whole fluid circulates in the same direction. This phenomenon causes the type of the fluid at a point to be replaced sequentially by time. This is well depicted in Figure 3. In Figure 3(a), the black and white fluids are separated initially and the black type fluid is at the right side of the chamber. As the mixing progresses in time, the black particles are moved upward and white particles are moved downward by the stirrers (Figure 3(g)). Furthermore, Figure 3(g) clearly shows that due to the mass diffusion, the concentration of black fluid (color intensity) is diminished as it arrives at the left side of the chamber and vice versa for the white fluid. Since the mixing index is a standard deviation from the mean value of the concentration, and the concentration of both white and black particles behaves similarly, the substitution of two fluids in a location within the chamber results in several local maxima, the mixing index of which is diminished by time.

In order to have an estimation of mixing efficiency in the whole domain, we take an average of mixing indices at ten control points. The overall mixing index is shown in Figure 5 for three stirrer angular velocities of $\omega = 200$, 400 and 600 rpm. As can be seen in this figure, the overall mixing index monotonically decreases with time for all rotational speeds, but, by increasing the angular velocity, a homogenous mixture is achieved within a shorter time interval as expected. It is also noted that the mixing process is accomplished twice as fast for the case of $\omega = 600$ rpm compared to $\omega = 200$.

3.2.2. Second rotation arrangement

For the second arrangement, the first and third row of the stirrers rotate counter clockwise while the middle

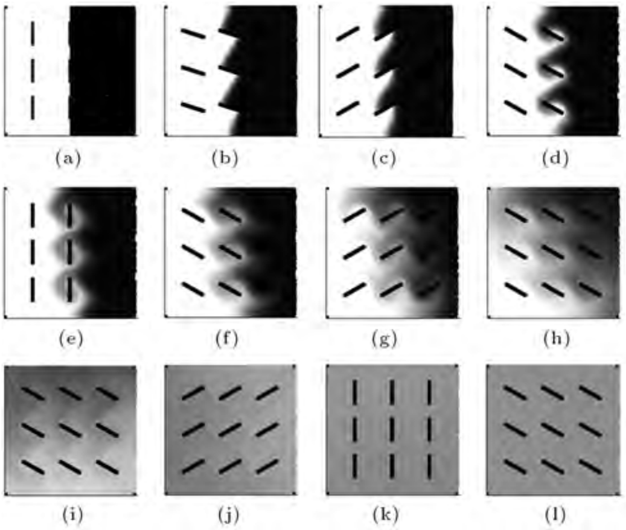

Figure 3. Model of the mixing chamber and the first arrangement at $\omega = 200$ rpm: (a) - (l) Concentration distribution at $t = 0$, 0.06 s, 0.1 s, 0.2 s, 0.3 s, 0.5 s, 1 s, 2 s, 5 s, 10 s, 15 s and 20 s, respectively.

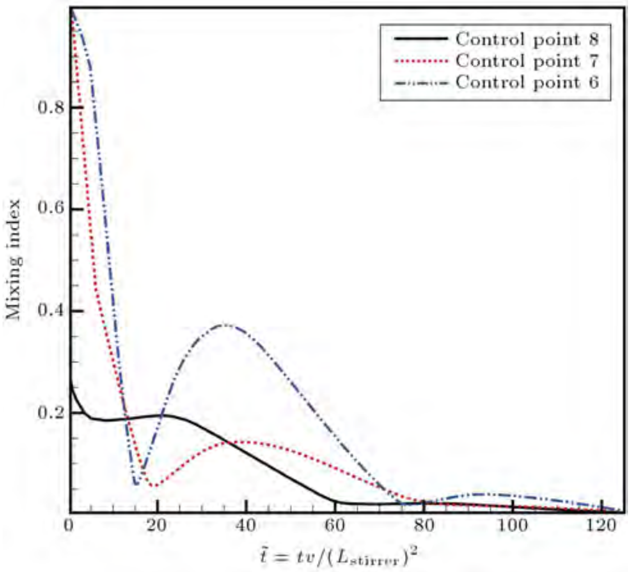

Figure 4. Comparison of mixing indices for the first rotation arrangement; $\omega = 200$ rpm for control points 6, 7 and 8 in the mixing chamber.

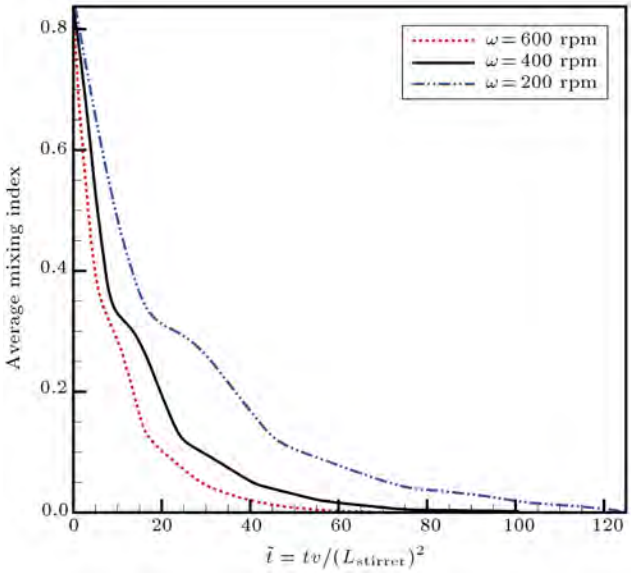

Figure 5. Comparison of overall mixing index for the first rotation arrangement; $\omega = 200$, 400 and 600 rpm.

row stirrers rotate clockwise. Two different simulations are conducted to show the effect of the second mixing arrangement in the chamber. For the first simulation (Figure 6, column A), the actual mass diffusivity of fluids is used and for the second simulation (Figure 6, column B), the mass diffusivity of two component is set to zero. Figure 6 shows the particle concentration in the chamber at different times for an angular velocity of $\omega = 400$ rpm. Here, the red color particles represent $C = 0$, the blue particles have the concentration value of $C = 1$ and the green particles represent the mixed fluid with $C = 0.5$. Since no molecular diffusion exists between the particles for case B, the particles retain their initial color, and Figure 6 (column B) only shows the dispersion of particles in the chamber as a result of convection.

As the concentration contours in Figure 6 (column A), illustrate, the flow field in this arrangement is quite different from the first arrangement. The mixing process in this arrangement also proceeds faster than the first case. The variation of the mixing index for three control points, 6, 7 and 8, is shown in Figure 7. The mixing index graphs decline sharply to the value of 0.2 for all three points before $3\tilde{t}$. In contrast to the first rotation arrangement, the substitution of two fluids does not occur at these control points and, therefore, a harmonic behavior is not observed, as in the previous case.

3.2.3. Third rotation arrangement

Finally, in the last rotation arrangement, the upper row of microstirrers rotate counter clockwise and the two lower rows rotate clockwise. The mixing time and overall mixing index in this case are very close to the previous case. The comparison between the overall mixing index of the three rotation arrangements in the angular velocity of $\omega = 400$ rpm is presented in Figure 8. The flow field disturbances generated by the microstirrer in the second arrangement cause maximum mixing efficiency compared with the two other cases. The mixing process reaches an acceptable mixing quality after about $20\tilde{t}$ for the first arrangement at $\omega = 400$ rpm, while the process time is reduced to

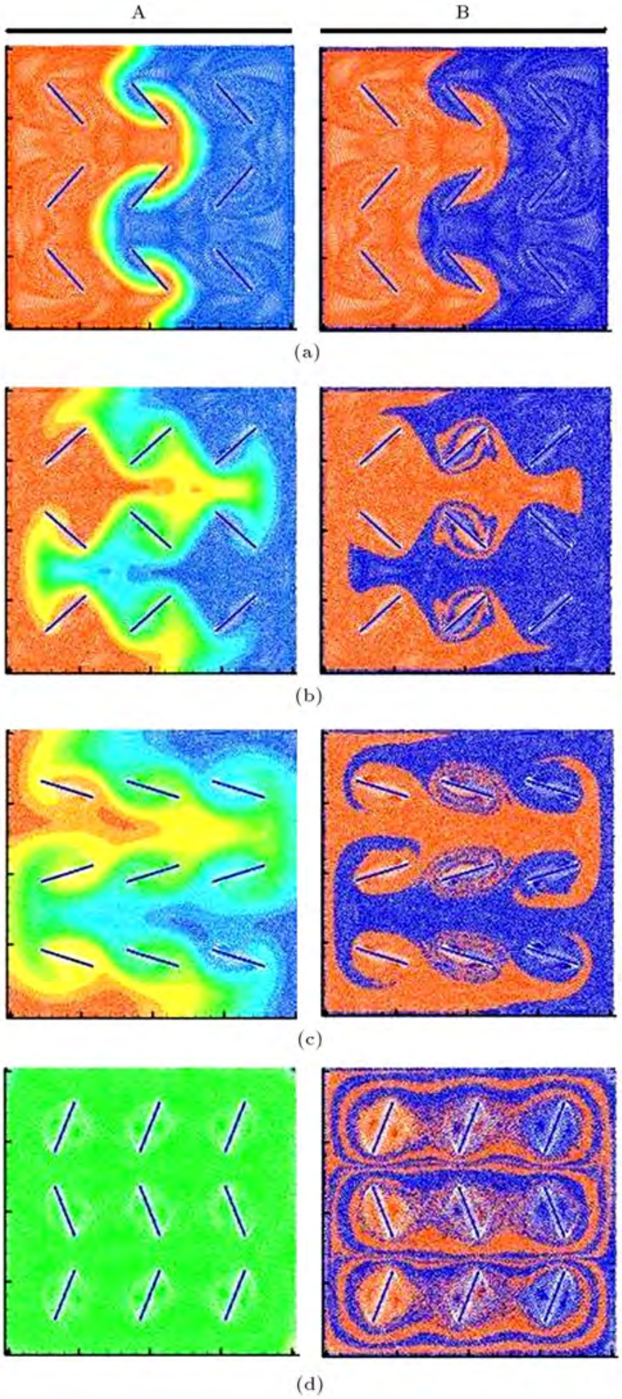

Figure 6. Model of the mixing chamber and the second arrangement at $\omega = 400$ rpm: (a)-(d) Concentration distribution at $t = 0.02$, 0.08, 0.25, 1.8.

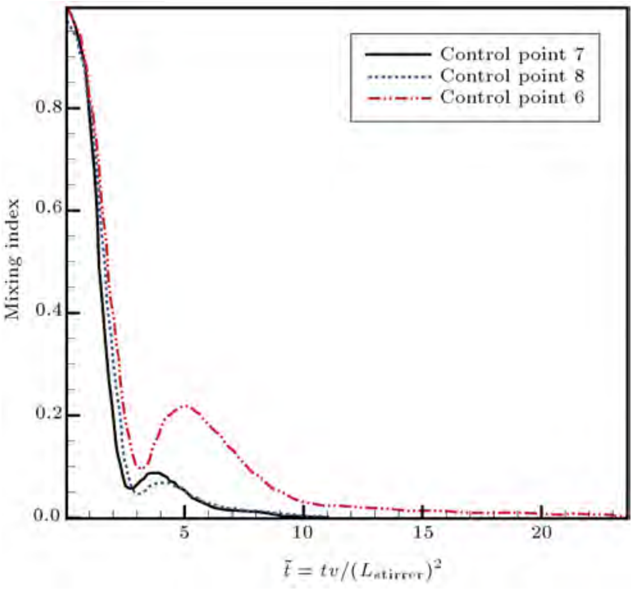

Figure 7. Comparison of mixing indices in control points 6, 7 and 8 in the mixing chamber, second rotation arrangement.

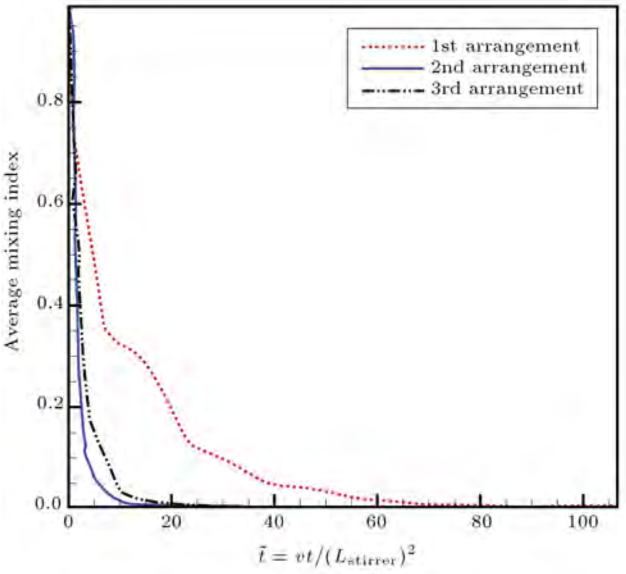

Figure 8. Comparison of mixing indices for three rotation arrangement, $\omega = 400$.

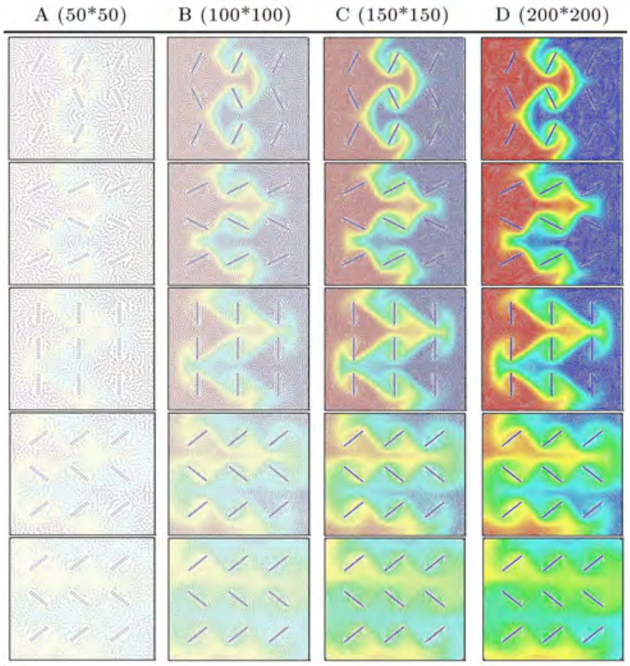

Figure 9. The convergence behavior for four number of particles. Column A: 2500 particles, Column B: 10000 particles; Column C: 22500 particle; Column D: 40000 particles.

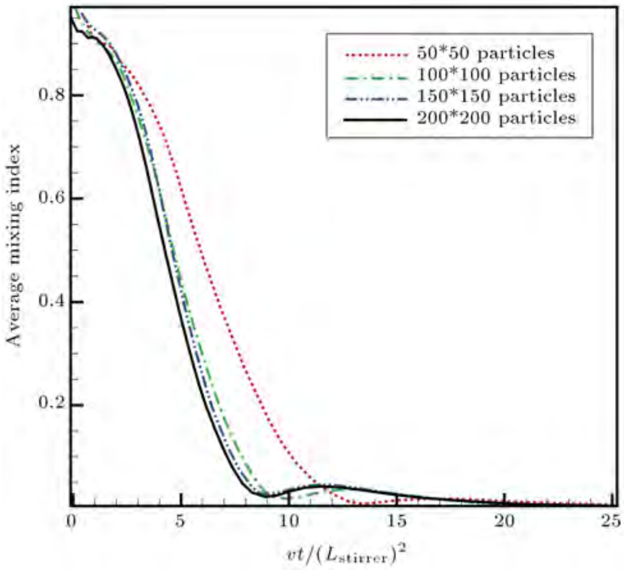

Figure 10. Comparison between the average mixing indices for four number of particles.

less than $3\tilde{t}$ in the second and third arrangements. This shows that a significant improvement can be expected by optimizing the rotation arrangement.

With regards to the convergence problem, in the classic CFD methods, a grid study is usually performed to show that the results do not depend on the number of nodes. Here, the mixing chamber with the second arrangement rotation was considered, and four different numbers of particles were used to study convergence behavior. The obtained results for concentration contours are shown in Figure 9 for 50*50 (column A), 100*100 (column B), 150*150 (column C) and 200*200 (column D) particles. As shown in this figure, by increasing the number of particles from 2500 to 40000, convergence is almost achieved on the third grid.

The comparison between the average mixing index and the mixing index at control point 6 for these four cases is also presented in Figures 10 and 11. The figures illustrate that the mixing parameters on these four grids are converged to the same value.

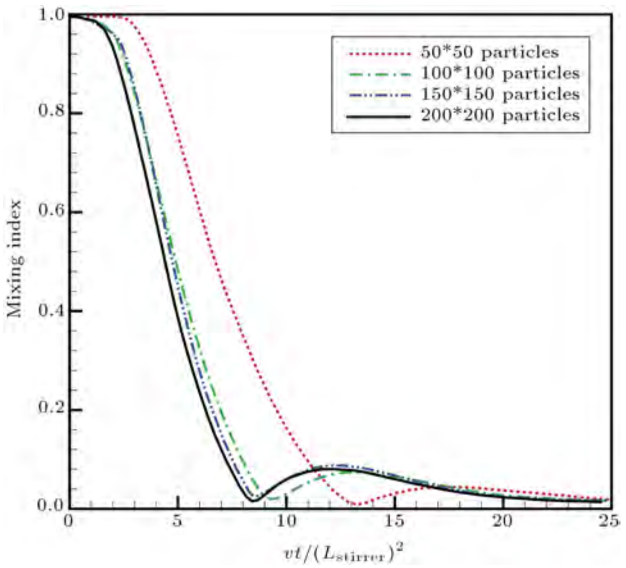

Figure 11. Comparison between the mixing indices in control point 6 for four number of particles.

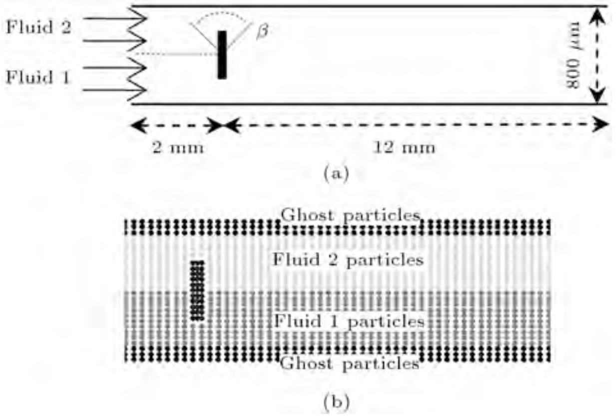

(a)

(b)

Figure 12. (a) Schematic of the microstirrer in a horizontal micromixer. (b) Arrangement of the SPH particles in the modeling of the horizontal micromixer.

3.3. Horizontal micromixer

In this section, a horizontal micromixer with inlet and outlet flow is modeled. The schematic configuration of this micromixer is presented in Figure 12(a). Two streams of different fluids are entered into a micro channel from the left and mixed with each other by the rotation of a microstirrer placed at the centerline of the microchannel.

The microchannel walls are modeled using mirror ghost particles (Figure 12(b)). Thus, no slip and no penetration boundary conditions are satisfied on the walls. Furthermore, virtual particles are used to simulate the microstirrer. 7000 fluid particles and 42 virtual particles are used for simulation of the fluid and microstirrer in the microchannel, respectively. The fluid particles are distributed in a uniform rectangular grid with 350 × 20 particles. Three columns of virtual particles are located in the microchannel and simulate the microstirrer rotation movement. The initial spacing between the particles are $dx = dy = 4 \times 10^{-5}$ and the time step size is $dt = 10^{-5}$. In order to find the effects of different parameters on mixing efficiency, the influence of the channel Reynolds number, the angular velocity of the microstirrer, the rotation or the oscillation movement of the microstirrer and the length of the microstirrer is explored. The mixing index calculated in cross sections downstream of the stirrer is considered as the performance criteria.

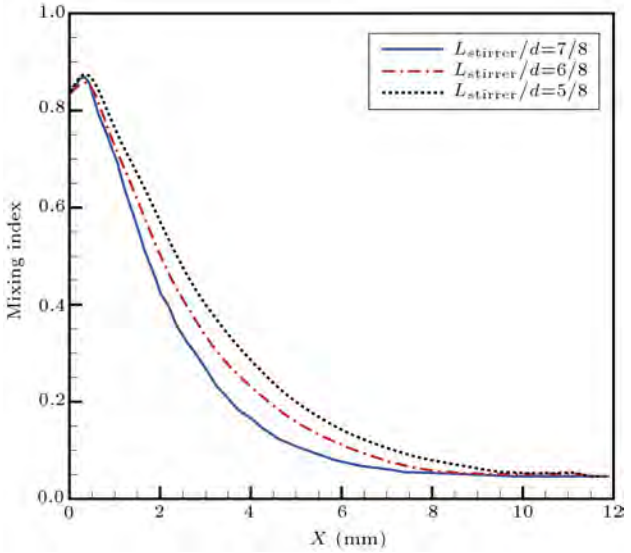

Figure 13. Comparison of mixing index for different length of the microstirrer at $\omega = 400$ rpm and Re = 1.

3.3.1. Effects of microstirrer length

First, the influence of microstirrer length in a range of $5/8 \leq L/d \leq 7/8$ is investigated. The mixing index for three different lengths of stirrer at Re = 1 and $\omega = 400$ rpm is calculated. As Figure 13 illustrates, since a longer microstirrer induces greater disturbances downstream of the channel, by increasing the length of the stirrer, the mixing process is accomplished within a shorter channel length.

3.3.2. Effects of inlet Reynolds number

The other prominent factor in the mixing efficiency of an active micromixer is the inlet Reynolds number. For this reason, the mixing index for Re = 1, 5, 10, 30, 50 and 100 is evaluated along the microchannel. The Peclet number for this problem is very large (in the order of $\text{Pe} \approx O(10^4)$) and the molecular diffusion has a negligible effect. Therefore, the mixing process is carried out by chaotic advection induced by the microstirrer. Figure 14 shows the concentration contours for the different inlet Reynolds numbers. As shown in the figure, mixing has been performed more appropriately at lower Reynolds number, and the required channel length for the complete mixing of the

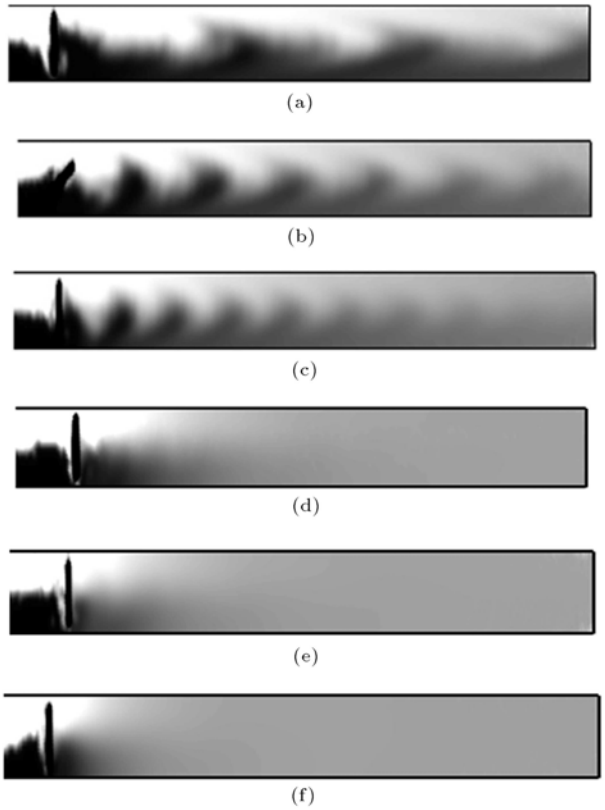

Figure 14. Concentration contours for $\omega = 400$ rpm: (a) Re = 100; (b) Re = 50; (c) Re = 30; (d) Re = 10; (e) Re = 5; and (f) Re = 1.

two streams increases considerably by increasing the Reynolds number.

In order to quantify the effect of the inlet Reynolds number on the required channel length for achieving complete mixing, the mixing index along the microchannel is calculated and illustrated in Figure 15 at six different inlet Reynolds numbers. As seen in this figure, the required channel length at Re = 10 is almost twice as long as its value for Re = 1. In fact, by decreasing the inlet Reynolds numbers, the Struhal number becomes higher, and, as a result, the microstirrer has more time to disturb the flow field and make the two fluids mix. On the other hand, for Re = 100 and 50, the mixing indices never reach 0.2 at the end of the channel, which shows that a longer channel is required for these cases. Furthermore, the mixing index shows oscillatory behavior at higher inlet Reynolds numbers. The appearance of oscillations can be justified by the fact that, at higher Reynolds number, a vortex stream is formed downstream of the microstirrer, as shown in Figure 14. As one may notice, the oscillations are reduced at Re = 30 and completely vanish for the lower inlet Reynolds numbers, Re = 10, 5 and 1.

3.3.3. *Effects of angular velocity*

The effects of the microstirrer angular velocity on the mixing process are investigated by performing a parametric study for Re = 1 and angular velocities of $\omega = 200$, 400 and 600 rpm. Figure 16 shows the mixing index along the channel for these angular velocities. As seen in this figure, by increasing the angular velocity, and, as a consequence, the Struhal number, disturbances generated by stirring are increased, which leads to a higher mixing efficiency in the micromixer. It is interesting to note that at $\omega = 600$, the mixing index of 0.2 is achieved in half the microchannel length required by $\omega = 200$.

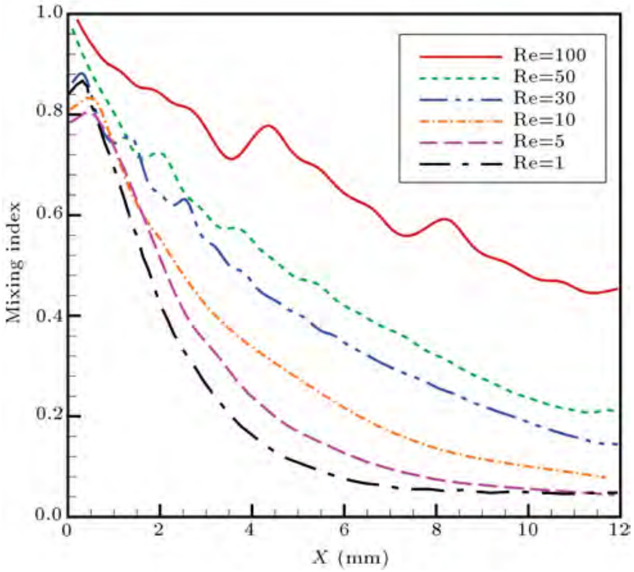

Figure 15. Comparison of the mixing indices for different entrance Re numbers.

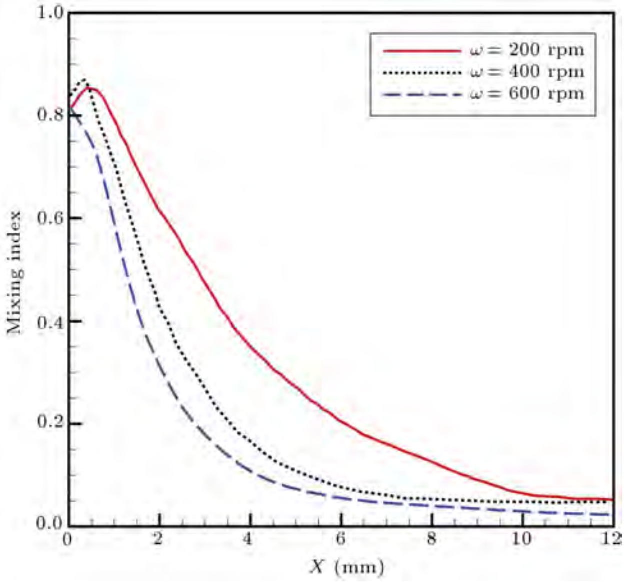

Figure 16. Comparison of the mixing indices for different angular velocities in Re = 1.

3.3.4. *Effects of microstirrer oscillation angle*

We assume that the stirrer oscillates with a specified angle, β, as shown in Figure 12(a) instead of rotating.

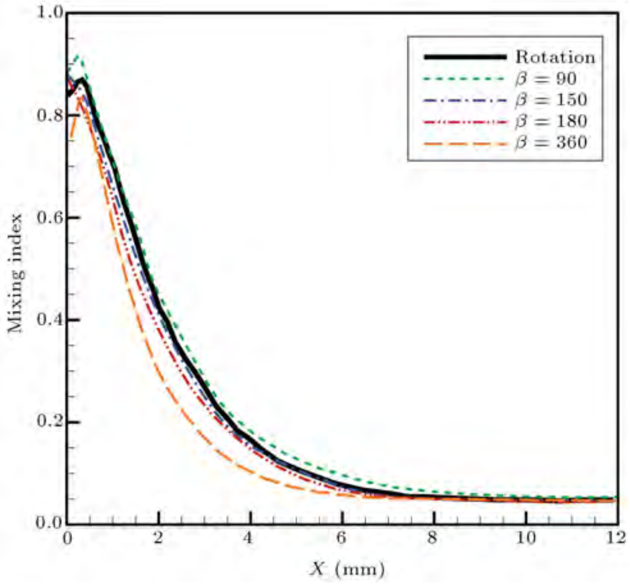

Figure 17. Comparison of the mixing indices for different oscillation angles in Re = 1.

The mixing process for four oscillation angles, $\beta = 90^\circ$, 150°, 180° and 360°, is simulated. In Figure 17, the variation of mixing index along the channel is illustrated for a rotating stirrer and four oscillating stirrers for $\omega = 400$ rpm and Re = 1. Although the mixing index is not considerably different for these cases, by increasing the oscillation angle, mixing efficiency is increased slightly. It is interesting to note that the rotating stirrer result is nearly close to the results of lower oscillating angles of the microstirrer. The Struhal and the entrance Reynolds numbers are similar for all cases. This observation proves that mixing efficiency is not affected significantly by the different modes of stirrer movement, as long as the other parameters, such as angular velocity and inlet Reynolds number, are restricted to constant values.

3.3.5. *Effects of inlet angle*

Finally, in the last case, the effects of inlet stream angle on mixing performance are investigated. As Figure 18 shows, this micromixer has two entrances and the microstirrer is located below the junction. Two fluids, which are water with different colors, similar to the previous cases, enter the mixing region through these two entrances, which have an angle of θ with the horizontal axis.

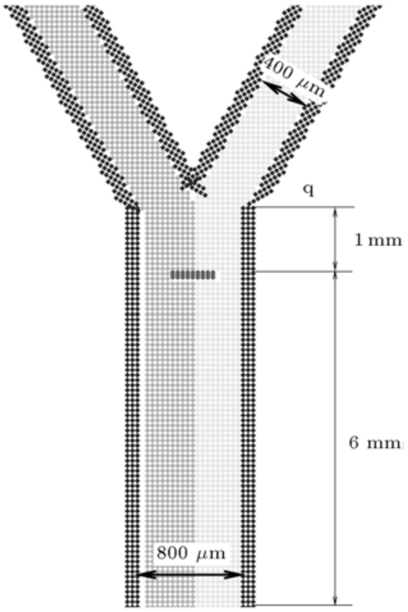

Figure 18. Schematic of an active Y shape micromixer and the arrangement of the SPH particles in the modeling.

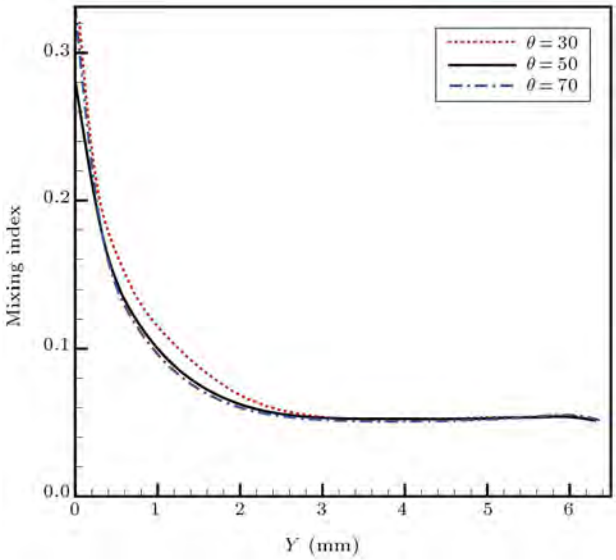

Figure 19. Comparison of mixing indices for Y-shape micromixer for different entrance angles.

In this simulation, the Reynolds number of flow is 1 and the angular velocity of the microstirrer is set to $\omega = 400$ rpm. Figure 19 depicts the variation of the mixing index along the channel for $\theta = 30^\circ$, 50° and 70°. As shown in this figure, the value of mixing indices is much less than the same condition for the horizontal micromixer, and for all three angles, the mixing indices reach 0.2 in only about 0.4 mm downstream of the microstirrer. Actually, when two streams of flow enter the channel with a different angle, their inertia causes some disturbance to develop at the interface of the two fluids, while this phenomenon does not exist in the horizontal micromixer. As Figure 19 shows, the mixing index at $Y = 0$ mm is about 0.3, which demonstrates that the two streams are approximately mixed before they reach the stirrer, and under the stirrer effect, the mixing intensifies downstream in a short length. On the other hand, in the horizontal micromixer, the mixing index of the mixture before the stirrer is about 0.8 at $X = 0$ mm, which illustrates that the two fluids are totally unmixed when they reach the stirrer.

It is also interesting to note that for the Y-shape micromixer, the effect of the stirrer is stronger than the horizontal micromixer. As Figures 19 and 13 illustrate, the slope of the mixing index in the horizontal micromixer is much less than the Y-shaped micromixer. For example, the mixing index is decreased from 0.3 to 0.2 in only about 0.2 mm in the Y-shaped micromixer, while it needs about 2 mm in the horizontal one.

To summarize, the inlet angle has a profound effect on mixing efficiency. However, by increasing the inlet angle, θ, only small improvement can be achieved in mixing efficiency.

4. Conclusion

In this work, the smoothed particle hydrodynamics method is used for modeling the flow field and diffusion phenomenon of two miscible fluids in active micromixers. The SPH method is found to be a robust numerical method in modeling complex geometries, moving boundaries and molecular diffusion. In the first case study, a 2D mixing chamber with nine microstirrers was simulated, and the effect of rotation arrangement and angular velocity on mixing efficiency was investigated. It was observed that the rotation arrangement is an effective parameter in mixing efficiency. It was shown that when the middle row stirrers rotate in a reverse direction, the mixing time reduces to one third of the initial arrangement. In the case of a horizontal micromixer, the influence of design parameters, such as angular velocity, inlet Reynolds number, rotation or oscillation movement of the microstirrer and length of the microstirrer, was studied. The mixing efficiency was calculated for Re = 1, 5, 10, 30, 50 and 100. It was concluded that by decreasing the inlet Reynolds number, the mixing efficiency is improved, as expected. Also, by increasing the angular velocity of the microstirrers, better mixing efficiency is achieved at the end of the microchannel. In addition, the effect of microstirrer length was explored and it was shown that by increasing the length, the micromixer has a better mixing performance, while the microstirrer mode of motion (oscillation or rotation) is not an effective parameter. Finally, in the last case study, the Y-shaped active micromixer was simulated and the influence of entrance angle was studied. It was found that the Y-shaped micromixers have much better efficiency than the horizontal micromixers and, also, by increasing the entrance angle, mixing efficiency is improved slightly. Since, in this study, equations were considered in two dimensional space, obtained results cannot be extended quantitatively to the problems with strong 3D effects. Especially, for cases in which the depth of the mixing chamber or the mixing channel is much larger than the thickness of the microstirrer, these effects are more prominent. Therefore, the result of this simulation is applicable when the dimensions of microchannel depth and micromixer thickness have nearly the same value, and where the 3D effects are negligible.

References

1. Rayes, D.R., Iossifidis, D., Auroux, P.A. and Manz, A. "Micro total analysis systems: 1. Introduction, theory and technology", *Anal. Chem.*, **74**, pp. 2623-2636 (2002).
2. Auroux, P.A., Iossifidis, D., Rayes, D.R. and Manz, A. "Micro total analysis systems: 2. Analytical standard operation and applications", *Anal. Chem.*, **74**, pp. 2637-52 (2002).
3. Chow, A.W. "Lab on a chip: opportunities for chemical engineering", *AIChE J.*, **48**, pp. 1590-1595 (2002).
4. Hessel, V., Loʿwe, H. and Schoʿnfeld, F. "Micromixers: a review on passive and active mixing principles", *Chem. Eng. Sci.*, **60**, pp. 2479-2501 (2005).
5. Chen, C.K. and Cho, C.C. "A combined active/passive scheme for enhancing the mixing efficiency of microfluidic devices", *Chemical Engineering Science*, **63**, pp. 3081-3087 (2008).
6. Park, J.M., Kim, D.S., Kang, T.G. and Kwon, T.H. "Improved serpentine laminating micromixer with enhanced local advection", *Microfluid. Nanofluid.*, **4**, pp. 513-523 (2008).
7. Glatzel, T., Litterst, C., Cupelli, C., Lindemann, T., Moosmann, C., Niekrawietz, R., Streule, W., Zengerle, R. and Koltay, P. "Computational Fluid Dynamics (CFD) software tools formicrofluidic applications - A case study", *Computers & Fluids*, **37**, pp. 218-235 (2008).
8. Tofteberg, T., Skolimowski, M., Andreassen, E. and Geschke, O. "A novel passive micromixer: lamination in a planar channel system", *Microfluid. Nanofluid.*, **8**, pp. 209-215 (2010). doi: 10.1007/s10404-009-0456-z)
9. Cortes-Quiroz, C.A., Zangeneh, M. and Goto, A. "On multi-objective optimization of geometry of staggered herringbone micromixer", *Microfluid. Nanofluid.*, **7**, pp. 29-43 (2009).
10. Chen, Z., Bown, M.R., O'Sullivan, B., MacInnes, J.M., Allen, R.W.K., Mulder, M., Blom, M. and van'tOever, R. "Performance analysis of a folding flow micromixer", *Microfluid. Nanofluid.*, **6**, pp. 763-774 (2009).
11. Tung, K.Y. and Yang, J.T. "Analysis of a chaotic micromixer tracking and FRET", *Microfluid. Nanofluid.*, **5**, pp. 749-759 (2008).
12. Kang, T.G., Singh, M.K., Kown, T.H. and Anderson. P.D. "Chaotic mixing using periodic and aperiodic sequences of mixing protocols in a micromixer", *Microfluid. Nanofluid.*, **4**, pp. 589-599 (2008).

13. Nguyen, N.T. and Wu, Z.G. "Micromixers-a review", *J. Micromech. Microeng.*, **15**, pp. R1-R16 (2005).

14. Koch, M., Witt, H., Evans, A.G.R. and Brunnschweiler, A. "Improved characterization technique for micromixer", *J. Micromech. Microeng.*, **9**, pp. 156-158 (1999).

15. Muller, S.D., Mezic, I., Walther, J.H. and Koumoutsakos, P. "Transverse momentum micromixer optimization with evolution strategies", *Computers & Fluids*, **33**, pp. 521-531 (2004).

16. Park, J.Y., Kim, Y.D., Kim, S.R., Han, S.Y. and Maeng, J.S. "Robust design of an active micro-mixer based on the Taguchi method", *Sencors and Actuators B*, **29**, pp. 790-798 (2008).

17. Lu, L.H., Suk, K. and Liu, C. "A magnetic microstirrer and array for microfluidic mixing", *J. Microelecteromechanical Systems*, **11**, pp. 462-469 (2002).

18. Wang, Y., Zhe, J., Chung, B.T.F. and Dutta, P. "A rapid magnetic particle driven micromixer", *Microfluid. Nanofluid.*, **4**, pp. 375-389 (2008).

19. Liu, G.R. and Liu, M.B. "Smoothed particle hydrodynamics a mesh free particle method", *World Scientific* (2005).

20. Lucy, L.B. "A numerical approach to the testing of the fission hypothesis", *Astron J.*, **83**, pp. 1013-1024 (1977).

21. Gingold, R.A. and Monaghan, J.J. "Smoothed particle hydrodynamics: Theory and application to nonspherical stars", *MonNot R Astron. Soc.*, **181**, pp. 375-89 (1977).

22. Schoenberg, I.J. "Contributions to the problem of approximation of equidistant data analytic function", *Q. Appl. Math*, **4**, p. 45 (1946).

23. Ferrari, A., Dumbser, M., Toro, E.F. and Armanini, A. "A new 3D parallel SPH scheme for free surface flows", *J. Computers and Fluids*, **38**, pp. 1203-1217 (2009).

24. Espanol, P. and Revenga, M. "Smoothed dissipative particle dynamics", *Pysical Review*, **67**, p. 026705 (2003).

25. Monaghan, J.J. "Simulating free surface flows with SPH", *J. Comput. Phys.*, **110**, pp. 399-406 (1994)

26. Morris, J.P., Fox, P.J. and Zhu, Y. "Modeling low Reynolds number incompressible flows using SPH", *J. Comp. Phys.*, **136**, pp. 214-226 (1997).

27. Monaghan, J.J. "Heat conduction with discontinuous conductivity", *Applied Mathematics Reports and Preprints*, Monash University, Melbourn, Australia (1995).

28. Batchelor, G.K., *An Introduction to Fluid Dynamics*, Cambridge Univ. Press. Cambridge, UK (1967).

29. Monaghan, J.J. "Smoothed particle hydrodynamics", *Rep. Prog. Phys.*, **68**, pp. 1703-1759 (2005).

30. Federico, I., Marrone, S., Colagrossi, A., Aristodemoa, F. and Antuonoc, F. "Simulating 2 Dopen-channel flows through an SPH model", *European Journal of Mechanics B/Fluids*, **34**, pp. 35-46 (2012).

Biographies

Ali Jafarian was born in 1984, in Iran. He received his BS degree in Fluid Mechanics from Semnan University and his MS in Thermo Fluids from Isfahan University of Technology, where he is currently a PhD student in the Thermo Fluid Division within the Mechanical Engineering Department. His major research interests include computational methods for multi-disciplinary flow, especially compressible multi phase flow and mesh free methods.

Ahmadreza Pishevar, PhD, DIC, received his PhD in Aeronautical Engineering from Imperial College, London, in 1996. Since 1997, he has been a Faculty Member of the Department of Mechanical Engineering at Isfahan University of Technology. He leads a research group focusing on Simulating Complex Phenomena in Thermo-Fluid Sciences, such as the Behavior of Condensed Matter under Impact and Shock Induced Loading, Meso-Scale Simulation of Electrokinetic and Colloid Transport Phenomena and the study of Multiphase Problems including Phase Change. He is now Chief Editor of the Journal of Numerical Methods in Engineering, published in Persian.

Mohammad Said Saidi is Professor of Mechanical Engineering at Sharif University of Technology, Iran. His research interests are Modeling and Numerical Analysis of Transport and Deposition of Aerosol Particles, Modeling and Numerical Analysis of Biofluids, Modeling and Numerical Analysis of Thermal-Hydraulics of Porous Media and Microchannels.